

GRAVITATIONAL RECOIL FROM SPINNING BINARY BLACK HOLE MERGERS

FRANK HERRMANN, IAN HINDER, DEIRDRE SHOEMAKER¹, PABLO LAGUNA²
Center for Gravitational Wave Physics,
The Pennsylvania State University, University Park, PA 16802, USA

RICHARD A. MATZNER
Center for Relativity and Department of Physics
The University of Texas at Austin, Austin, Texas 78712, USA
Draft version August 14, 2018

ABSTRACT

The inspiral and merger of binary black holes will likely involve black holes with both unequal masses and arbitrary spins. The gravitational radiation emitted by these binaries will carry angular as well as linear momentum. A net flux of emitted linear momentum implies that the black hole produced by the merger will experience a recoil or kick. Previous studies have focused on the recoil velocity from unequal mass, non-spinning binaries. We present results from simulations of equal mass but spinning black hole binaries and show how a significant gravitational recoil can also be obtained in these situations. We consider the case of black holes with opposite spins of magnitude a aligned/anti-aligned with the orbital angular momentum, with a the dimensionless spin parameters of the individual holes. For the initial setups under consideration, we find a recoil velocity of $V = 475 \text{ km s}^{-1} a$. Supermassive black hole mergers producing kicks of this magnitude could result in the ejection from the cores of dwarf galaxies of the final hole produced by the collision.

Subject headings: black hole physics — galaxies: nuclei — gravitation — gravitational waves — relativity

1. INTRODUCTION

There is ample observational evidence that supermassive black holes (SMBHs) are common at the centers of galaxies (Richstone et al. 1998; Magorrian et al. 1998), with masses in the range $10^5 - 10^9 M_{\odot}$. These SMBHs are involved in exciting astrophysical phenomena. For instance, there is a remarkable, not completely understood, correlation between the velocity dispersion of the bulge of the host galaxy and the mass of the SMBH (Ferrarese & Merritt 2000). There is also indication of a correlation of the mass of the SMBH with the mass of the host dark matter halo (Ferrarese 2002). An interesting aspect of SMBH growth arises as a consequence of hierarchical cold dark matter cosmologies, in which large-scale structures are formed by mergers. SMBHs would then grow both by gas accretion and by coalescence with other SMBHs (brought together when their host galaxies collide (Volonteri et al. 2003; Begelman et al. 1980)). The work in this paper focuses on one aspect of the merger of SMBHs, the kick in the final SMBH.

The late inspiral and merger of SMBHs produces extremely energetic gravitational radiation, which will be observable by the planned space-based gravitational wave antenna LISA (Danzmann 2003; Prince 2003). Gravitational radiation produced during the inspiral and merger of black holes (BHs) not only carries energy with it, but, except in special-symmetry cases, can also

transport net linear and angular momentum. For instance, in the merger of unequal mass SMBHs, a net flux of linear momentum will be emitted by the system (Peres 1962; Bekenstein 1973). As a consequence, the final BH will experience a gravitational recoil or kick. There are observations that hint at such scenarios, in which a SMBH has been ejected in an ongoing galaxy merger (Haehnelt et al. 2006). (An alternative explanation could be that the ejection is due to gravitational slingshot of three or more SMBHs in the merger.) It is then very important to get good estimates of recoil velocities in BH mergers. These estimates have a profound effect on the understanding of the demographics of SMBHs at the cores of galaxies, their growth (Haiman 2004) and their merger rates (Micic et al. 2006). Knowledge of the conditions under which kicks are produced could also help explain the absence of massive BHs in dwarf galaxies and stellar clusters (Madau & Quataert 2004; Merritt et al. 2004), and could determine the population of BHs in the interstellar and intergalactic medium.

Gravitational recoil estimates of unequal mass binaries have been addressed using both analytic and full numerical relativity approaches. The first quasi-Newtonian analytic studies (Fitchett 1983; Fitchett & Detweiler 1984) produced kick velocities as large as $\sim 1500 \text{ km s}^{-1}$. Wiseman (1992) and more recently Blanchet et al. (2005) and Damour & Gopakumar (2006) improved these estimates by including post-Newtonian (PN) effects. The maximum kick in these studies was found to be in the range of $\sim 74 - 250 \text{ km s}^{-1}$, and it occurred for $\eta \sim 0.2$, where $\eta \equiv M_1 M_2 / (M_1 + M_2)^2$ is the symmetrized mass ratio parameter. (This corresponds to a mass ratio $q \equiv M_1 / M_2 \sim 0.38$.) These analytic PN studies also showed that the final value of the kick is mostly

¹ IGPG, Department Physics, The Pennsylvania State University, University Park, PA 16802, USA

² IGPG, Departments of Astronomy & Astrophysics and Physics, The Pennsylvania State University, University Park, PA 16802, USA

accumulated during the merger or plunge phase of the binary. Since the plunge phase is beyond the limit of applicability of PN approximations, the results can only be taken as “best-bet estimates” (Damour & Gopakumar 2006).

There are two semi-analytic studies that in principle had a better handle on the plunge phase. Campanelli (2005) obtained kick velocities of $\sim 300 \text{ km s}^{-1}$ using the *Lazarus* approach, a framework (Baker et al. 2002) that combines full numerical relativity and close-limit approximation (CLA) perturbation theory (Price & Pullin 1994). More recently, Sopuerta et al. (2007) and Sopuerta et al. (2006) combined PN estimates during the inspiral with kick estimates using the CLA. The maximum recoil obtained in this work was $\sim 167(1 + e) \text{ km s}^{-1}$, with e the eccentricity of the binary. Finally, full numerical relativity studies have also been carried out by Herrmann et al. (2006), Baker et al. (2006) and Gonzalez et al. (2006). Only full numerical relativity approaches provide accurate estimates of kicks since they correctly handle the non-linear behavior of the plunge. The most comprehensive study so far is that by Gonzalez et al. (2006), in which a maximum kick velocity of $\sim 175 \text{ km s}^{-1}$ was obtained also for $\eta \sim 0.2$ ($q \sim 0.38$), consistent with PN studies. What is interesting is that the findings of Sopuerta et al. (2007) based on the CLA are remarkably close to the full numerical relativity results by Gonzalez et al. (2006), supporting the view that the kick is mostly due to the linear momentum emitted during the plunge, where the CLA has been demonstrated to provide a good approximation (Anninos et al. 1995). To our knowledge, the only kick study involving spinning BHs is that by Favata et al. (2004). They considered the case of an extreme-mass-ratio system with a spinning SMBH. Using BH perturbation theory they estimated kick velocities of $\sim 100 - 200 \text{ km s}^{-1}$. Head-on collisions of spinning BHs have also been recently considered (Choi 2007).

To help us understand *our* computational results, we present next a rough order-of-magnitude estimate of the kicks one should expect. Note first that there must be some asymmetry between the BHs in order for there to be asymmetric radiation which can lead to kicks. Thus, in the non-spinning case, unequal masses are required; here we consider binaries of equal masses, but different spin (magnitude or direction). The kick is expected to increase as the relevant spin increases, but especially symmetric cases will still show zero kick (e.g. when the BHs have their spins aligned parallel to the orbital angular momentum). The order-of-magnitude estimate can be obtained from the radiative linear momentum loss formula (Thorne 1980; Kidder 1995a). Excluding non-spin terms, this formula reads

$$\begin{aligned} \frac{dP^i}{dt} &= \frac{16}{45} \epsilon^{ijk} I_{jl}^{(3)} H_{kl}^{(3)} + \frac{4}{63} H_{ijk}^{(4)} H_{jk}^{(3)} \\ &+ \frac{1}{126} \epsilon^{ijk} I_{jlm}^{(4)} H_{klm}^{(4)}. \end{aligned} \quad (1)$$

Here I_{ij} and I_{ijk} are respectively the mass quadrupole and octupole. Similarly, H_{ij} and H_{ijk} are the spin quadrupole and octupole, respectively. In (1), a super-index (n) denotes an n th-time derivative. Clearly equation (1) predicts a periodic force for exactly circular or-

bits. As the BHs spiral together the strength of the periodic kick increases, so we estimate the kick from the last half orbit before merger.

Consider a binary system consisting of BHs in circular orbit with equal masses ($M_1 = M_2 = M/2$). In the absence of spin this would produce no kick, but here we set data with each BH having spin perpendicular to the orbit, the spins oppositely directed, each with dimensionless Kerr spin parameter a ($0 \leq a \leq 1$). This is the configuration we use below for our computational evaluation of the kick. The calculation of the mass quadrupole is familiar, and for circular orbits in the xy plane with orbital angular velocity ω and coordinate separation d gives nonzero values:

$$\begin{aligned} I_{xx}^{(3)} &= 2M d^2 \omega^3 \sin(2\omega t) \\ I_{xy}^{(3)} &= -2M d^2 \omega^3 \cos(2\omega t) \\ I_{yy}^{(3)} &= -2M d^2 \omega^3 \sin(2\omega t). \end{aligned} \quad (2)$$

The spin quadrupole can be most easily calculated by imagining a spin dipole (charges $\pm M/2$, separation $aM/2$) and conceptually taking the limit at the end. The result is

$$\begin{aligned} H_{xz}^{(3)} &= \frac{1}{4} M^2 d a \omega^3 \sin(\omega t) \\ H_{yz}^{(3)} &= -\frac{1}{4} M^2 d a \omega^3 \cos(\omega t). \end{aligned} \quad (3)$$

Inserting (2) and (3) into the first term in equation (1) gives

$$\begin{aligned} \frac{dP^x}{dt} &= \frac{8}{45} M^3 d^3 a \omega^6 \sin(\omega t) \\ \frac{dP^y}{dt} &= -\frac{8}{45} M^3 d^3 a \omega^6 \cos(\omega t). \end{aligned} \quad (4)$$

Notice that the force is in the plane of the orbit and rotates with the orbit. The average over half a cycle is $2/\pi$, so equation (4) is a good estimate for any half cycle as the orbit spirals in. The total force can then be approximated as

$$\frac{dP}{dt} = \frac{16}{45\pi} M^3 d^3 a \omega^6. \quad (5)$$

Compare this to the total luminosity:

$$\frac{dE}{dt} = \frac{2}{5} M^2 d^4 \omega^6. \quad (6)$$

Thus the asymmetry in radiation that contributes to the kick is

$$\frac{dP}{dE} = \frac{dP/dt}{dE/dt} = \frac{4aM}{9\pi d}, \quad (7)$$

which is ~ 0.02 for dimensionless spin parameter $a \sim 1/2$ and $d \sim 6M$. (The latter is an estimate of the separation near the “last orbit”.) If ΔE is the total energy radiated by the binary, an estimate of the (half orbit) kick is

$$\begin{aligned} V &\sim c \left(\frac{dP}{dE} \right) \left(\frac{\Delta E}{M} \right) \\ &\sim 300 \text{ km s}^{-1} \left(\frac{dP/dE}{0.02} \right) \left(\frac{\Delta E/M}{0.05} \right). \end{aligned} \quad (8)$$

For another estimate, we note that Favata et al. (2004) specialized the PN equation (3.31) in Kidder

(1995b) to the case of circular orbit with spins parallel and anti-parallel to the orbital angular momentum. The resultant kick velocity is given by

$$V = V_q + 883 \text{ km s}^{-1} \left(\frac{f_{SO}(q, a_1, a_2)}{f_{SO, \max}} \right) \left(\frac{2M}{r_{\text{term}}} \right). \quad (9)$$

Above V_q is the contribution to the kick that depends only on the mass ratio q ; this contribution vanishes for equal mass binaries ($q = 1$). The radius r_{term} is the separation at which gravitational radiation terminates. The scaling function in equation (9) is given by $f_{SO}(q, a_1, a_2) = q^2(a_2 - qa_1)/(1+q)^5$ with $f_{SO, \max} = f_{SO}(1, \pm 1, \mp 1) = 1/16$. Therefore, for the cases we have investigated, equation (9) reduces to $V = 883 \text{ km s}^{-1} a (2M/r_{\text{term}})$, comparable to our estimate above, for reasonable choices of r_{term} .

There is another effect similar to the pulsar kick mechanism described by Harrison & Tademaru (1975). It involves explicit retardation effects (so is not captured in the multipole expression of equation (1)), and gives estimates of similarly sized kicks. We shall see that full numerical relativity simulations give comparable kicks to this estimate.

The paper is organized as follows: In Sec. 2, we present the computational methodology and details of how the initial data were constructed. Sec. 3 gives details of the method to estimate kicks. Code tests and a convergence analysis are given in Sec. 4. The gravitational recoil estimates are presented in Sec. 5, with conclusions given in Sec. 6.

2. COMPUTATIONAL METHODOLOGY AND INITIAL DATA

The numerical simulations of binary black holes (BBH) in our work were obtained following the *Moving Puncture Recipe* (MPR). The essence of this recipe is: (A) a particular formulation of the Einstein field equations and (B) a set of coordinate or gauge conditions for updating field variables during evolution as well as for handling the BH singularities. The form of the evolutions required by the MPR is the so-called BSSN 3+1 formulation of Einstein's equations (Nakamura et al. 1987; Shibata & Nakamura 1995; Baumgarte & Shapiro 1999). A derivation of the BSSN equations and a few examples of their applications can be found in the review by Baumgarte & Shapiro (2003).

In addition to the form of the evolution equations, the success of the MPR is due to the coordinate or gauge conditions (Alcubierre et al. 2003; Baker et al. 2006b; Campanelli et al. 2006a). The MPR gauge conditions are equations that determine the lapse function α and the shift vector β^i . The lapse is a ‘‘local’’ measure of proper time, and the shift vector encapsulates the freedom of labeling events at a given time (Baumgarte & Shapiro 2003). The explicit form of the evolution equations for the lapse and shift in the MPR are $\partial_0 \alpha = -2\alpha K$ and for the shift $\partial_0 \beta^i = 3/4 B^i$ and $\partial_0 B^i = \partial_0 \tilde{\Gamma}^i - \xi B^i$, where $\partial_0 = \partial_t - \beta^j \partial_j$. K is the trace of the extrinsic curvature, $\tilde{\Gamma}^i$ is the trace of the conformal connection and $\xi = 2$ is a free dissipative parameter. The importance of these gauge conditions is twofold: first, they avoid the need of excising the BH singularity from the computational domain since they effectively halt the evolution

TABLE 1
INITIAL DATA PARAMETERS

Model	x/M	P/M	S/M^2	m_1/M	m_2/M	E/M
S0.05	2.95	0.13983	0.05	0.4683	0.4685	0.98445
S0.10	2.98	0.13842	0.10	0.4436	0.4438	0.98455
S0.15	3.05	0.13547	0.15	0.3951	0.3953	0.98473
S0.20	3.15	0.13095	0.20	0.2968	0.2970	0.98499

(i.e. the lapse function α vanishes) near the BH singularity (Hannam et al. 2006). Second, they allow for movement of the BH or *puncture* throughout the computational domain while freezing the evolution inside the BH horizon.

The code used for this work was produced by the *Kranc* code generation package (Husa et al. 2006), the *Cactus* infrastructure (Cactus 2007) for parallelization and *Carpet* (Schnetter et al. 2004) for mesh refinement. The code is based on fourth order accurate finite differencing of spatial operators and uses 4th order Runge-Kutta for time integration with a Courant factor of 0.5.

The initial data use punctures (Brandt & Brüggmann 1997) to represent BHs. In Einstein's theory, initial data are not completely freely specifiable; they must satisfy the Hamiltonian and momentum constraints. We use the spectral code developed by Ansorg et al. (2004) to solve these constraints. The initial free-data (e.g. angular momentum, spins, masses, separations) are chosen according to the effective potential method (Cook 1994; Baumgarte 2000). This method yields BBH initial data sets representing BBHs in quasi-circular orbit. In general terms, the effective potential method consists of minimizing the ‘‘binding energy’’ of the binary to determine the BBH parameters.

Table 1 contains the BBH parameters of our simulations. The BHs are located at positions $(\pm x/M, 0, 0)$, have linear momentum $(\pm P/M, 0, 0)$, spin $(0, 0, \pm S/M^2)$ and bare puncture masses $m_{1,2}/M$, with $M = M_1 + M_2$ the total mass of the binary. Notice that the bare puncture masses are slightly different. The reason for this difference is because of the spin contribution to the mass of each hole (measured from the area of their apparent horizons); in order to keep the individual masses of the BHs, M_1 and M_2 , equal, (slight) adjustments to the bare masses are necessary. The configurations are such that the total angular momentum is for all cases $J/(\mu M) = 3.3$ with $\mu = M_1 M_2 / (M_1 + M_2)$. It is important to notice that S is not the Kerr spin parameter $0 \leq a_{Kerr} \leq m_{BH}$ typically associated with rotating BHs. The dimensionless spin parameter for each BH is given by $a_{1,2} = S/M_{1,2}^2$ with $M_{1,2} = M/2$. The cases considered here, $S/M^2 = \{0.05, 0.10, 0.15, 0.20\}$, correspond to $a = \{0.2, 0.4, 0.6, 0.8\}$, respectively. For reference, the total ADM mass E/M in the initial data is also reported in Table 1.

The computational grids consist of a nested set of 10 refinement levels, with the finest mesh having resolution $h = M/40$. This resolution translates into a resolution of about $h = m/19 - m/12$, with respect to the bare mass m of the puncture according to Table 1. The minimal resolution found to be adequate for spinning cases according to Campanelli et al. (2006b) is $h < M/30$. In our $h = M/40$ simulations there are 4 refinement levels

of 58^3 grid-points nested within 6 levels of 102^3 grid-points. During the evolution the shape and number of grid-points per refinement level vary as the centers of the grids track the positions of the black holes. The coarsest mesh is kept fixed and extends to $650M$ from the origin in each direction.

3. GRAVITATIONAL RECOIL

The gravitational recoil is computed from the rate of change of linear momentum

$$\frac{dP^i}{dt} = \lim_{r \rightarrow \infty} \left\{ \int \frac{d^2E}{d\Omega dt} n^i r^2 d\Omega \right\}, \quad (10)$$

which is determined by the fluxes of energy E and linear momentum P^i (n^i is the unit normal to the sphere). In order to compute the recoil velocity, the Newtonian momentum relation is used, $V^i = P^i/M$.

In terms of Ψ_4 , the component of the Weyl curvature tensor representing outgoing radiation, equation (10) reads (Newman & Tod 1980)

$$\frac{dP^i}{dt} = \lim_{r \rightarrow \infty} \left\{ \frac{1}{4\pi} \int \left| \int_{-\infty}^t \Psi_4 dt' \right|^2 n^i r^2 d\Omega \right\}. \quad (11)$$

Equation (11) is applied at a finite radius $r > 30M$ away from the “center of mass” of the binary but far enough from the boundary of the computational domain to avoid the effects from spurious reflection from the boundary (Zlochower et al. 2005). The Weyl scalar Ψ_4 is computed in the bulk of the computational domain and is then projected onto the sphere and used in the computation of equation (11).

We also estimate the gravitational recoil using a mode decomposition. Instead of constructing Ψ_4 in the bulk of the computational domain and interpolating it on a sphere to be used in equation (11), we decompose Ψ_4 into spin-weight -2 spherical harmonics and then compute the recoil. That is, one first constructs the coefficients ${}_{-2}C_{\ell m}$ such that

$$\Psi_4 = \sum_{\ell m} {}_{-2}C_{\ell m}(t, r) {}_{-2}Y_{\ell m}(\theta, \varphi). \quad (12)$$

Given these coefficients, the gravitational recoil is given by

$$\frac{dP^i}{dt} = \sum_{\ell m \bar{\ell} \bar{m}} \langle \ell, m | \bar{\ell}, \bar{m} \rangle \quad (13)$$

where $\langle \ell, m | \bar{\ell}, \bar{m} \rangle$ represents the contribution to dP^i/dt from the overlap

$$\langle \ell, m | \bar{\ell}, \bar{m} \rangle \propto \text{Re} \left[-{}_2\hat{C}_{\ell m}^* - {}_2\hat{C}_{\bar{\ell} \bar{m}} \int n^i {}_{-2}Y_{\ell m}^* {}_{-2}Y_{\bar{\ell} \bar{m}} d\Omega \right], \quad (14)$$

with ${}_2\hat{C}_{\ell m} \equiv \int_{-\infty}^t {}_2C_{\ell m} dt'$. This mode-overlap decomposition has the advantage that the contribution from different overlapping modes can be studied individually.

There is an important issue to keep in mind when using both equations (11) and (13) to estimate kicks. It is well known that initial data in BBH simulations contain spurious radiation. Fortunately, this radiation does not seem to have a significant effect on the dynamics of

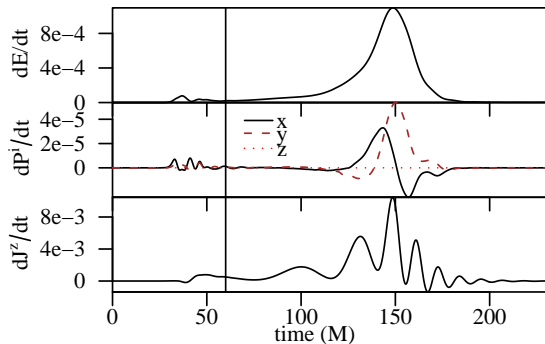


FIG. 1.— Fluxes of energy dE/dt , linear momentum dP^i/dt and angular momentum dJ/dt as a function of time for the $S0.10$ ($a = 0.4$) case. The vertical line at $60M$ denotes t_{\min} , the lower limit of the time integration used to estimate kicks which avoids contamination from the spurious radiation in the initial data.

the binary. However, because of the time-integration involved in the kick formulas, the estimates are affected by the spurious radiation. To alleviate this problem, we set the lower limit in the time integral to be t_{\min} and choose t_{\min} as the time after which the spurious burst has passed. As an example, Figure 1 displays the fluxes of energy dE/dt , linear momentum dP^i/dt and angular momentum dJ/dt through the detector at $r_{\text{det}} = 30M$ for the $S0.10$ case. It is clear from these rates that there is a spurious burst from the initial data for $t < 50M$. In particular, notice the effect on dP^i/dt at early times. The line at $t_{\min} = 60M$ shows our choice for this cut-off. The precise choice of t_{\min} is not important, as long as the initial spurious burst is eliminated and t_{\min} is not too close to the time when the amplitude of the gravitational wave becomes relevant. Since we use several locations (“detectors”) at different radii to compute fluxes, the value of t_{\min} is adjusted as $t_{\min} = 30M + r_{\text{det}}$, where r_{det} denotes the detector radius. Note the smallness of dP^i/dt from Figure 1. It translates to velocities of $\sim 0.2 \text{ km s}^{-1}$; thus, we will not plot V^z in subsequent figures.

Another important check when computing kicks using equations (11) and (13) is the dependence of the results on the extraction radius r_{det} . The kick formulas are in principle valid in the limit $r \rightarrow \infty$, but one applies them at a finite extraction radius r_{det} where there is sufficient resolution. Figure 2 shows the recoil velocity as a function of time computed at different detector radii, $r_{\text{det}}/M = (30, 40, 50)$. The time dependence of the velocities has not been adjusted by the lag in arrival times at each detector. Although small, one can see from Figure 2 that there is a slight sensitivity of the extracted kick velocity to the location of the detector for the ranges we considered. This variation is within the error estimates of our kicks. The origin of this dependence of the extracted kick on the detector location could be numerical (e.g. outer boundary, mesh refinement interfaces, etc.) or due to the redshift and tail effects.³

4. CODE TESTS AND WAVEFORM CONVERGENCE

We have tested that our code produces a sufficient level of convergence for equal mass, non-spinning BH binaries that we are confident in the results. In particular, we have carried out extensive tests (Shoemaker et al. 2007)

³ We thank the anonymous referee for bringing this to our attention.

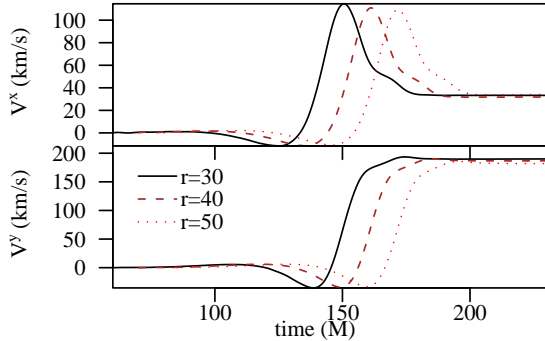


FIG. 2.— Recoil velocity V^x and V^y computed from different detector locations for $S0.10$ with resolution $h = M/40$. The detectors were located at $r_{\text{det}}/M = (30, 40, 50)$.

for the $R1$ run in Baker et al. (2006a) and found resolution ranges that yield between 3rd- and 4th- order convergence. Also as a code test, we carried out a non-spinning, unequal mass simulation for $\eta = 0.23$. The kick obtained from this run ($\sim 130 \text{ km s}^{-1}$) matches that by Gonzalez et al. (2006). Because the BBH setups in our present work have no symmetries, the computational cost of each simulation is high (for our $h = M/40$ resolution runs the cost is ~ 44 hours on 32 CPU cores for a total of about ~ 1400 CPU hours on a supercomputer), so to demonstrate convergence our runs were limited to resolutions $h \leq M/40$. We present convergence results for the $S0.10$ case; the other cases have similar behavior.

Figure 3 shows the amplitude of the dominant $\ell = 2, m = 2$ mode of Ψ_4 . The top panel of the figure displays the mode at the three different resolutions ($h/M = 1/32, 1/35, 1/40$), while the bottom panel shows the coarse-medium (“c-m”) differences and the medium-fine (“m-f”) differences rescaled for 2nd, 3rd and 4th order. As the plot shows, this mode converges between 3rd and 4th order. In our convergence studies for other systems (e.g. equal mass BHs) getting closer to 4th-order convergence required at least a factor of two between the coarsest and finest resolution. Given the range of resolutions that we are able to do for the present study, the deterioration of our convergence should not be surprising. Nonetheless, we believe that the observed level of convergence in our simulations will not affect the astrophysical implications of the magnitude of our kick estimates.

As a check of our implementation of the kick extraction, Figure 4 compares the recoil velocity computed from equation (11) and equation (13) for the case $S0.10$ with resolution $h = M/40$. For equation (13), we include up to $\ell = 4$ modes. It is evident from this plot that with the modes $\ell \leq 4$ one can reconstruct most of the total recoil velocity.

5. RESULTS

First, we present the main results of our work, namely the kick estimates together with the radiated energy and angular momentum, followed by a discussion of convergence and a mode analysis of the kicks.

5.1. Kicks and Radiated Energy and Momentum

The core results of our work are summarized in Table 2. Table 2 lists the values for the total recoil V , energy ΔE and angular momentum ΔJ radiated for each of the cases considered. The reported values were obtained

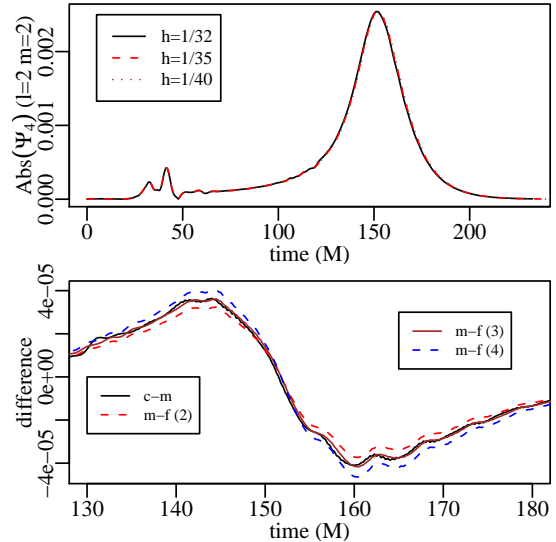


FIG. 3.— The amplitude of the dominant $\ell = 2, m = 2$ mode of Ψ_4 for the case $S0.10$ ($a = 0.4$). The top plot shows the mode at three different resolutions ($h/M = 1/32, 1/35, 1/40$), while the bottom shows the small differences between the medium-coarse (“c-m”) and the medium-fine (“m-f”) simulations rescaled for 2nd, 3rd and 4th order. The waveform is between 3rd- and 4th-order convergent.

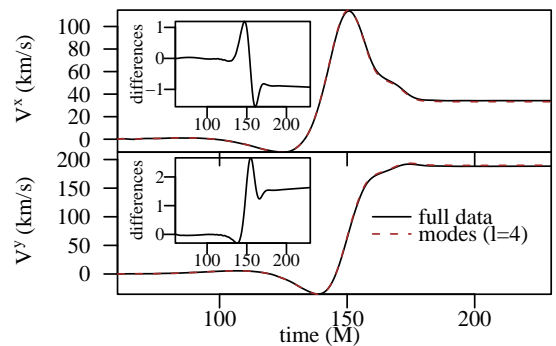


FIG. 4.— Recoil velocity V^x and V^y versus time computed from equation (11) and equation (13) for the $S0.10$ model with resolution $h = M/40$ extracted at $r_{\text{det}} = 30 M$. V^z is below 0.2 km/s and hence is not shown. The insets labeled “differences” show the difference between the recoil from equation (11) and equation (13) with modes up to and including $\ell = 4$

TABLE 2
RADIATED QUANTITIES

Model	a	$V(\text{km s}^{-1})$	$\Delta E(\%)$	$\Delta J(\%)$
S0.05	0.2	96 ± 7	3.24	26.82
S0.10	0.4	190 ± 10	3.30	27.05
S0.15	0.6	285 ± 12	3.33	27.12
S0.20	0.8	392 ± 33	3.34	26.83

with resolutions $h = M/40$ and extracted at $r_{\text{det}} = 40 M$. For reference, we include also the dimensionless spin parameter a . Figure 5 displays the recoil velocity V as a function of the dimensionless spin parameter a for all the resolutions used in our simulations. Solid circles denote resolutions $h = M/40$, diamonds resolutions $h = M/32$ and inverted triangles resolutions $h = M/30$. The error

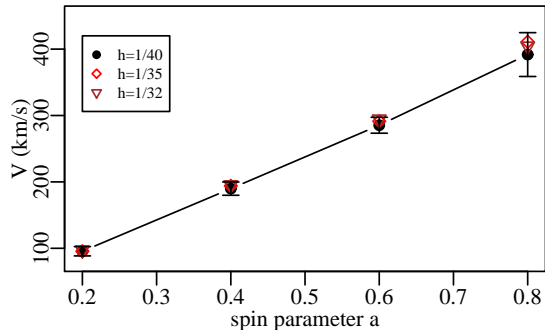


FIG. 5.— Magnitude of the recoil velocity V as a function of the dimensionless spin parameter a . Solid circles are for resolutions $h = M/40$, diamonds for resolutions $h = M/32$ and inverted triangles for resolutions $h = M/30$. In each case, the results at different resolution cluster more tightly than the conservatively estimated error bars (Table 2).

bars correspond to the conservatively estimated errors listed in Table 2, and are larger than the actual scatter of the results at different resolution.

In order to estimate these errors, for each spin case, we perform Richardson error estimates of the total recoil velocity V assuming 2nd order convergence. We then increase these errors to take into account factors such as the deterioration of convergence in the weak mode-overlaps (see below). We believe these are conservative best-guess errors that could be reduced with, among other things, higher resolution.

Note in Figure 5 the linear dependence of the magnitude of the kick velocity V on the spin parameter, as expected from the multipole example in Section 1. A fit to the data yields $V = 475 \text{ km s}^{-1} a$.

An interesting aspect of the spin configuration we have considered is the fraction of radiated energy ΔE and angular momentum ΔJ . The fraction radiated is approximately constant within the accuracy of our simulations. One possible reason why ΔE and ΔJ do not seem to depend on the spins of the holes could be due to the set up of our initial data. By construction, the four cases we considered have the same total initial angular momentum $J/\mu M = 3.3$. In our case with spins oppositely directed and with equal magnitude the variations in the total ADM energy are $< 0.05\%$, as can be seen from Table 1.

5.2. Mode Analysis and Convergence

With the kick formula (13), we were able to investigate the contribution of each mode-overlap $\langle \ell, m | \bar{\ell}, \bar{m} \rangle$ to the total recoil velocity. Figure 6 shows the contribution that each mode-overlap makes to the total kick velocity for the $S0.10$ case with $h = M/40$ resolution. The mode-overlaps have been sorted from largest to smallest. The total recoil is labeled with an inverted triangle. Positive mode-overlap contributions are labeled with circles and negative with diamonds. There are two important points to take from this figure: A) Note how quickly the contribution to V^x and V^y from each mode-overlap falls off; that is, there are few mode-overlaps that have significant contribution. B) The two most dominant mode-overlaps $\langle 2, -2 | 2, -1 \rangle$ and $\langle 2, 2 | 2, 1 \rangle$ contribute almost equally 54% (note that other modes contribute negatively) in V^x and 40% in V^y .

Another way of showing the dominance of the

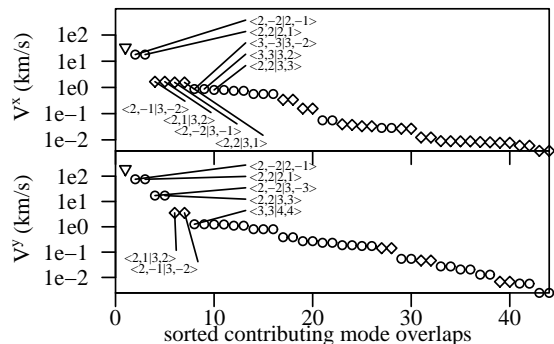


FIG. 6.— Contribution to the recoil velocity components V^x and V^y from each $\langle \ell, m | \bar{\ell}, \bar{m} \rangle$ mode-overlap for the $S0.10$ case with resolution $h = M/40$ extracted at $r_{det} = 30 M$. The recoil from combining all mode-overlaps is labeled with an inverted triangle. Positive mode-overlap contributions are labeled with circles and negative with diamonds.

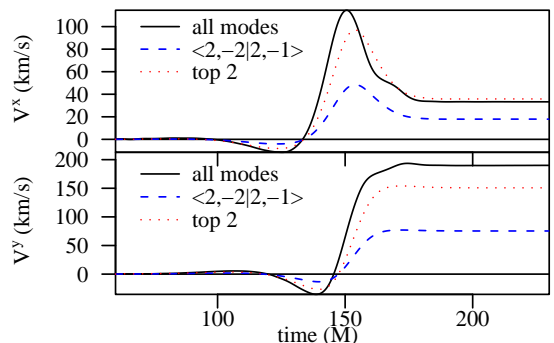


FIG. 7.— Recoil velocity components V^x and V^y versus time for the case $S0.10$ with resolution $h = M/40$ extracted at $r_{det} = 30 M$. The solid line gives the accumulation in time of recoil from all mode-overlaps combined, dotted line denotes the combined accumulations of only the two most dominant mode-overlaps, $\langle 2, -2 | 2, -1 \rangle$ and $\langle 2, 2 | 2, 1 \rangle$, and the dashed line the accumulation in time of the $\langle 2, -2 | 2, -1 \rangle$ mode overlap.

$\langle 2, -2 | 2, -1 \rangle$ and $\langle 2, 2 | 2, 1 \rangle$ mode-overlaps is presented in Figure 7. This figure shows the accumulated velocity as a function of time. The solid line gives the accumulation in time of recoil from all mode-overlaps combined, the dotted line shows the combined accumulations of the two most dominant mode-overlaps, $\langle 2, -2 | 2, -1 \rangle$ and $\langle 2, 2 | 2, 1 \rangle$, and the dashed line displays the accumulation in time of the $\langle 2, -2 | 2, -1 \rangle$ mode overlap.

Given that the mode-overlaps $\langle 2, -2 | 2, -1 \rangle$ and $\langle 2, 2 | 2, 1 \rangle$ are the principal contributors to the total kick velocity, we analyzed the convergence properties of these overlaps. Figure 8 displays the differences of the $\langle 2, -2 | 2, -1 \rangle$ mode-overlap from three resolutions, $h/M = (1/32, 1/35, 1/40)$. The solid line is the difference between the coarse and medium resolutions (“c-m”). The other lines show the difference between the medium and fine resolutions (“m-f”), scaled to match (“c-m”) for 3rd, 4th and 5th order convergence. It is clear from this figure that this mode-overlap is close to being 4th-order convergent. A similar situation occurs for the other dominant mode-overlap $\langle 2, 2 | 2, 1 \rangle$. Unfortunately, the situation is different for the other weaker mode-overlaps. These overlaps involve higher modes of Ψ_4 that are much more difficult to resolve given the range of resolutions we have. When these weaker modes are added to obtain the total recoil, one is no longer able to reach the desired 4th-order convergence. In some in-

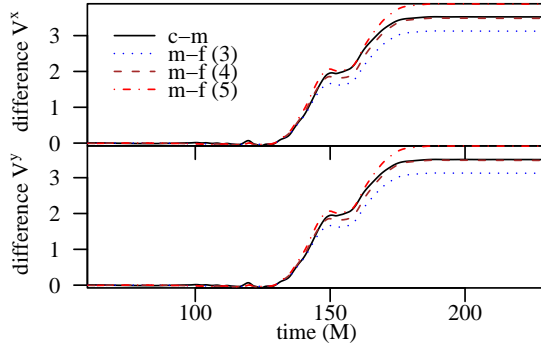


FIG. 8.— Convergence analysis of the recoil contribution from the dominant overlap $(2, -2|2, -1)$ for the S0.10 case extracted at $r_{det} = 30 M$. The solid line gives the difference between the coarse and medium resolutions (“c-m”). The other lines show the difference between the medium and fine resolutions (“m-f”), scaled to match (“c-m”) for 3rd, 4th and 5th order convergence.

stances it drops to 1st-order convergence. Fortunately, as we have seen from Figure 6, their contribution to the overall recoil is small. We are confident that our total kick velocities will not change significantly if one is able to achieve finer resolutions than $h = M/40$.

6. SUMMARY AND DISCUSSION

We have computed estimates of BH merger kick velocities from previously untreated physical effects arising from the spin of the holes. Our computational simulations provided firm predictions of kick velocities for BBH systems of equal mass and anti-aligned spins. Because we are able to accurately resolve the dominant modes that contribute to the kick and estimate those kicks by a number of methods, we are confident in our astrophysical conclusions involving the binary types we considered. Previous studies which considered the merger of (non-spinning) BHs of unequal masses produced kicks

⁴ Soon after the completion of our work, results that support our findings of spin effects on kicks were obtained by Campanelli et al.

$\sim 200 \text{ km s}^{-1}$ with a reasonably broad maximum near the symmetrized mass ratio of $\eta = 0.2$ (mass ratio 0.38). From the astrophysical point of view, 200 km s^{-1} is interesting. For instance, the escape velocity from the center of dwarf elliptical galaxies is 300 km s^{-1} , assuming the standard picture of dark matter halos. We found spin kick velocities $V = 475 \text{ km s}^{-1} a$, where a is the dimensionless spin parameter, in opposite-spin configurations (see Figure 5).

For black holes ($10 - 20 M_{\odot}$) seen in the galaxy, there are observations supporting spin parameters $a \gtrsim 0.8$ (McClintock et al. 2006), and theoretical explanations of why this is so are generally applicable to SMBHs also. Thus we expect substantial kicks due to spin interactions. Our simulations predict typical kicks $\gtrsim 400 \text{ km s}^{-1}$ in astrophysical BH mergers of all masses. These results could explain the observed absence of central black holes in dwarf elliptical galaxies. Our simulations show limitations, mostly due to the high cost of performing very high resolution runs. But, because we are able to accurately resolve the dominant modes that contribute to the kick, we believe that our astrophysical conclusions are secure⁴.

Thanks to José González, Ben Owen, Carlos Sopuerta, Ulrich Sperhake and Nico Yunes for helpful conversations. The authors acknowledge the support of the Center for Gravitational Wave Physics funded by the National Science Foundation under Cooperative Agreement PHY-0114375. This work was supported by NSF grants PHY-0354821 to Deirdre Shoemaker, PHY-0244788 and PHY-0555436 to Pablo Laguna and PHY-0354842 and NASA grant NNG 04GL37G to Richard Matzner. Computations were carried out at NCSA under allocation TG-PHY-060013N, and at the Texas Advanced Computation Center, University of Texas System.

(2007); Koppitz et al. (2007).

REFERENCES

- Alcubierre, M., Brügmann, B., Diener, P., Koppitz, M., Pollney, D., Seidel, E., & Takahashi, R. 2003, *Phys. Rev. D*, 67, 084023
- Anninos, P., Price, R. H., Pullin, J., Seidel, E., & Suen, W.-M. 1995, *Phys. Rev. D*, 52, 4462
- Ansorg, M., Brügmann, B., & Tichy, W. 2004, *Phys. Rev. D*, 70, 064011
- Baker, J., Campanelli, M., & Lousto, C. O. 2002, *Phys. Rev. D*, 65, 044001
- Baker, J. G., Centrella, J., Choi, D.-I., Koppitz, M., & van Meter, J. 2006a, *Phys. Rev. D*, 73, 104002
- . 2006b, *Phys. Rev. Lett.*, 96, 111102
- Baker, J. G., Centrella, J., Choi, D.-I., Koppitz, M., van Meter, J. R., & Miller, M. C. 2006, *ApJ*, 653, L93
- Baumgarte, T. W. 2000, *Phys. Rev. D*, 62, 024018
- Baumgarte, T. W. & Shapiro, S. L. 1999, *Phys. Rev. D*, 59, 024007
- . 2003, *Physics Reports*, 376, 41
- Begelman, M. C., Blandford, R. D., & Rees, M. J. 1980, *Nature*, 287, 307
- Bekenstein, J. D. 1973, *ApJ*, 183, 657
- Blanchet, L., Qusailah, M. S. S., & Will, C. M. 2005, *ApJ*, 635, 508
- Brandt, S. & Brügmann, B. 1997, *Phys. Rev. Lett.*, 78, 3606
- Cactus. 2007, <http://www.cactuscode.org>
- Campanelli, M. 2005, *Class. Quant. Grav.*, 22, S387
- Campanelli, M., Lousto, C. O., Marronetti, P., & Zlochower, Y. 2006a, *Phys. Rev. Lett.*, 96, 111101
- Campanelli, M., Lousto, C. O., & Zlochower, Y. 2006b, preprint (gr-qc/0604012)
- Campanelli, M., Lousto, C. O., Zlochower, Y., & Merritt, D. 2007, preprint (gr-qc/0701164)
- Choi, D. 2007, private communication
- Cook, G. B. 1994, *Phys. Rev. D*, 50, 5025
- Damour, T. & Gopakumar, A. 2006, *Phys. Rev. D*, 73, 124006
- Danzmann, K. 2003, *Advances in Space Research*, 32, 1233
- Favata, M., Hughes, S. A., & Holz, D. E. 2004, *Astrophys. J.*, 607, L5
- Ferrarese, L. 2002, *ApJ*, 578, 90
- Ferrarese, L. & Merritt, D. 2000, *ApJ*, 539, L9
- Fitchett, M. J. 1983, *MNRAS*, 203, 1049
- Fitchett, M. J. & Detweiler, S. 1984, *MNRAS*, 211, 933
- Gonzalez, J. A., Sperhake, U., Bruegmann, B., Hannam, M., & Husa, S. 2006, preprint (gr-qc/0610154)
- Haehnel, M. G., Davies, M. B., & Rees, M. J. 2006, *MNRAS*, 366, L22
- Haiman, Z. 2004, *ApJ*, 613, 36
- Hannam, M., Husa, S., Pollney, D., Brügmann, B., & O’Murchadha, N. 2006, preprint (gr-qc/0606099)
- Harrison, E. R. & Tademaru, E. 1975, *ApJ*, 201, 447
- Herrmann, F., Shoemaker, D., & Laguna, P. 2006, preprint (gr-qc/0601026)
- Husa, S., Hinder, I., & Lechner, C. 2006, *Computer Physics Communications*, 174, 983
- Kidder, L. E. 1995a, *Phys. Rev. D*, 52, 821
- . 1995b, *Phys. Rev. D*, 52, 821
- Koppitz, M. et al. 2007, preprint (gr-qc/0701163)
- Madu, P. & Quataert, E. 2004, *ApJ*, 606, L17

- Magorrian, J. et al. 1998, *Astron. J.*, 115, 2285
- McClintock, J. E., Shafee, R., Narayan, R., Remillard, R. A., Davis, S. W., & Li, L.-X. 2006, *ApJ*, 652, 518
- Merritt, D., Milosavljevic, M., Favata, M., Hughes, S. A., & Holz, D. E. 2004, *Astrophys. J.*, 607, L9
- Micic, M., Abel, T., & Sigurdsson, S. 2006, preprint (astro-ph/0609443)
- Nakamura, T., Oohara, K., & Kojima, Y. 1987, *Prog. Theor. Phys. Suppl.*, 90, 1
- Newman, E. T. & Tod, K. P. 1980, *General Relativity and Gravitation: One hundred years after the birth of Albert Einstein*, ed. A. Held, Vol. 2 (Plenum Press N.Y.), pp 1
- Peres, A. 1962, *Phys. Rev.*, 128, 2471
- Price, R. H. & Pullin, J. 1994, *Physical Review Letters*, 72, 3297
- Prince, T. 2003, *American Astronomical Society Meeting*, 202, 3701
- Richstone, D. et al. 1998, *Nature*, 395, 14
- Schnetter, E., Hawley, S. H., & Hawke, I. 2004, *Class. Quantum Grav.*, 21, 1465
- Shibata, M. & Nakamura, T. 1995, *Phys. Rev. D*, 52, 5428
- Shoemaker, D., Herrmann, F., Hinder, I., & Vaishnav, B. 2007, in preparation
- Sopuerta, C. F., Yunes, N., & Laguna, P. 2006, *Phys. Rev. D*, 74, 124010
- . 2007, *ApJ*, 656, L9
- Thorne, K. S. 1980, *Rev. Mod. Phys.*, 52, 299
- Volonteri, M., Haardt, F., & Madau, P. 2003, *ApJ*, 582, 559
- Wiseman, A. G. 1992, *Phys. Rev. D*, 46, 1517
- Zlochower, Y., Baker, J. G., Campanelli, M., & Lousto, C. O. 2005, *Phys. Rev. D*, 72, 024021